ELSEVIER

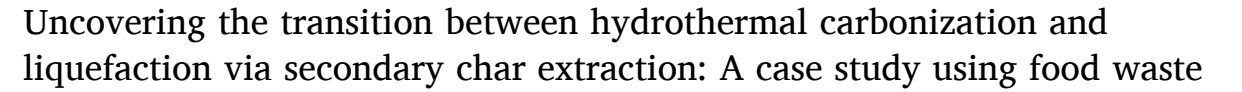
Contents lists available at ScienceDirect

Waste Management

journal homepage: www.elsevier.com/locate/wasman



Research Paper



Matteo Pecchi ^{a,b}, Marco Baratieri ^b, Alex R. Maag ^{a,c}, Jillian L. Goldfarb ^{a,*}

- ^a Department of Biological & Environmental Engineering, Cornell University, USA
- ^b Faculty of Science and Technology, Free University of Bolzano, Italy
- ^c Department of Chemical Engineering, Worcester Polytechnic Institute, Worcester, MA, USA

ARTICLE INFO

Keywords: Hydrothermal carbonization Hydrothermal liquefaction Secondary char Solvent extraction Food waste

ABSTRACT

Despite the ability to perform both processes in the same reactor, hydrothermal carbonization (HTC) and hydrothermal liquefaction (HTL) are considered two distinct processes differentiated by their reaction temperatures. As temperatures increase from the less severe HTC range into the HTL regime, the product distribution progressively favors an organic bio-oil phase relative to solid hydrochar. Solvents are commonly used to extract bio-oil from the solid residues produced during HTL, and to separate the amorphous secondary char from the coal-like primary char of HTC hydrochars. This suggests secondary char is a HTL biocrude precursor. Lipid-rich food waste was hydrothermally processed between 190 and 340 °C, spanning HTC to HTL conditions. Higher temperatures produce more gas, less liquid, and similar amounts of a progressively less oxygenated hydrochars, suggesting a gradual transition from HTC to HTL. However, analyses of ethanol-separated primary chars and secondary chars tell a different story. While the primary char is progressively more carbonized with temperature, the secondary char composition sharply changes at 250 °C. That is, lipid hydrolysis begins around 220 °C, but proceeds rather completely at 250 °C and above. A lower HTL temperature reduces the energy cost of the hydrothermal process, yet enables full lipid hydrolysis into long chain fatty acids while minimizing recondensation and repolymerization of fatty acids onto the primary char and their subsequent amidation. This maximizes the conversion of lipid-rich feedstocks into liquid fuel precursors with up to 70 % energy recovery.

1. Introduction

European food waste (FW) production reached 57 Mt y^{-1} in 2020, with about 41 Mt y^{-1} produced at the retail and household level (Eurostat, 2022). Across the Atlantic Ocean, the Environmental Protection Agency (EPA) estimates more than 100 Mt y^{-1} of FW were produced in the US in 2018, with 63 Mt y^{-1} produced at the retail and household level (EPA, 2018). For both Europe and the US, a large share of retail and household level FW—a heterogeneous mixture with relatively high energy and moisture content—is disposed of in landfills or incinerated, which leads to large greenhouse gas emissions (EPA, 2018; European Environment Agency., 2020).

The design of sustainable processes to valorize FW is complicated by its high moisture content, which renders thermal processes like combustion, gasification, and pyrolysis inefficient due to the increased energy requirements required to initially pre-dry the feed (Akbari et al., 2020; Özçimen et al., 2022). Hydrothermal conversion leverages the

water present in FW as a solvent medium for thermochemical transformation (Beims et al., 2020; Pauline and Joseph, 2020) without the need for a pre-drying phase (Lachos-Perez et al., 2022; Li et al., 2022). Hydrothermal carbonization (HTC) and hydrothermal liquefaction (HTL) convert heterogeneous wet organic mixtures into renewable solid and liquid fuels, respectively.

During HTC, the feedstock is heated in an aqueous environment under autogenous pressure to temperatures between 170 and $\sim 250\,^{\circ}\text{C}$, with residence times from minutes to hours. The main products of HTC are a solid hydrochar (HC), an aqueous phase, and a gaseous phase mainly composed of CO $_2$ (Lachos-Perez et al., 2022). During HTC, the elemental carbon content of the solid matrix increases with its aromatic content as a result of hydrolysis, dehydration, decarboxylation, and aromatization reactions (Zhuang et al., 2022). The residual carbon rich solid phase resulting from these reactions is termed primary char (PC). Additionally, char formation occurs via the recondensation of the organics from initial biomass hydrolysis that partition into the aqueous

E-mail addresses: JillianLGoldfarb@gmail.com, goldfarb@cornell.edu (J.L. Goldfarb).

^{*} Corresponding author.

phase and then redeposit onto the solid char via polymerization and condensation (Pecchi et al., 2022a). This tar-like phase often appears as micro-spheres that adhere to the solid PC matrix (Lucian et al., 2018). It is broadly termed secondary char, defined here as the fraction of HC that can be separated via solvent extraction (Lucian et al., 2018; Pecchi et al., 2022a).

HTL is performed at higher temperatures and pressures than HTC, usually between ~ 250 and $370\,^{\circ}\text{C}$ and between 7 and 25 MPa. These conditions maintain water in a subcritical state, yet the harsher environment enhances decomposition of the feedstock into soluble molecules, favoring the formation of liquid biocrude over HC (Zhuang et al., 2022). Some biocrude molecules undergo re-condensation and repolymerization (Yang et al., 2019) to form a viscous oily phase of hydrocarbons, aromatic and oxygenated compounds (Beims et al., 2020). Feedstock composition, temperature, heating rate, and residence time all influence the extent of feedstock conversion and relative solid and liquid yields, with the higher temperatures of HTL resulting in a lower solid HC yield as compared to HTC (Zhang et al., 2020).

HTC and HTL are usually investigated as distinct processes within discrete temperature regimes, even though (1) there is no universally identified temperature at which HTC transitions to HTL and (2) both processes proceed via the same initial reactions and yield similar products (albeit in varying amounts). The same solvents are often used to separate the products in both HTC (PC from SC) and HTL (HC and biocrude) (Li et al., 2020; Lucian et al., 2018; Xu and Savage, 2014). However, scant literature examines the shift in product distributions and characteristics between carbonization and liquefaction processes of the same feedstock. As such, we use a solvent extraction technique to assess the partitioning of products from HTC and HTL between the solid and oily phase across process regimes, providing fundamental information on the transition between these hydrothermal processes.

In prior work, we assessed the efficiency and selectivity of six different solvents to extract SC from HC (Pecchi et al., 2022a). The HC were produced by HTC at 250 $^{\circ}$ C, 1 h, of three different food waste materials, include the representative retail-level FW used for the present work. We found that alcohols extract the greatest amount of SC from high-lipid HCs (up to 50 % of the total HC as SC), including the FW mixture. Ethanol was the preferable solvent as it extracted the highest amount of volatile matter as SC (retaining fixed carbon in PC) and has a reduced hazard level as compared to methanol, which showed similar performance.

Leveraging this recently acquired knowledge, the present work uses ethanol extraction of SC to tackle a series of key questions, often overlooked, in hydrothermal processing research. Namely, is there an identifiable transition between HTC and HTL? If so, can this transition be observed by changes in SC to biocrude composition and yield? To answer these questions, FW is carbonized/liquefied spanning temperatures between 190 and 340 $^{\circ}$ C, and the obtained solid HC is extracted using ethanol. The primary and secondary char (or the residual char and the biocrude in the case of more severely processed FW) are then analyzed in terms of mass balance and composition to understand the nature of the transition between what are often considered two disparate processes despite their outward similarities. The findings from this new work could inform the selection of process conditions required for FW processing that balance desired product type, quality and yield. This could reduce overall HTC/HTL energy cost, hazard, and material losses for FW processing.

2. Materials and methods

All HTC and HTL experiments were performed on a representative retail-level FW which was synthesized and characterized as detailed in our previous study (Pecchi et al., 2022a). The feedstock mimics the typical food waste composition from large producers in the US and was compiled based on the ingredients and quantities indicated by (Buzby et al., 2014); the precise composition is available in the Supplemental

Information (SI). The FW was stored in the freezer prior to use. FW properties (on dry basis) are provided in Table 1; the FW as-received moisture content was 52.9 \pm 2.5 wt% as determined gravimetrically by drying to constant weight at 105 °C. A subset of experiments to study the transition behavior on a non-lipid feedstock used microcrystalline cellulose (Alfa Aesar, A17730); comprising 0.2 \pm 0.3 wt% ash, 92.9 \pm 0.6 wt% volatile matter, and 6.9 \pm 0.4 wt% fixed carbon.

2.1. HTC and HTL experiments

FW was hydrothermally processed using a 0.3 L stirred Parr HTL reactor. In each test, the reactor was loaded with 150 g of prepared FW and water necessary to obtain a 15 wt% dry solid loading and a reactor filling ratio of 0.5. Prior to starting a run, the reactor was purged 3 times with high-purity N2 (Airgas), pressurized to 0.55-0.58 MPa and stirred with an impeller at 400 rpm. The reactor was heated to either 190, 220, 250, 280, 310, or 340 $^{\circ}\text{C}$ and held for 1 h. Heating ramps lasted 18, 31, 40, 53, 66, and 104 min for each setpoint, respectively. The maximum pressure reached for each temperature is reported in the SI. After a 1hour reaction time, the reactor was quenched in an ice bath, reaching a temperature of <70 °C within 5 min. The headspace gas was purged in a fume hood when the reactor temperature was below 20 °C. The reactor contents were vacuum filtered through cellulose filter paper (Whatman, 0.45 μm) and the HC was oven-dried at 85 °C overnight and stored in plastic containers for further analyses. The test at 220 °C was triplicated to estimate error in the present work (additional replicates were run for prior extraction studies on the same biomass; see (Pecchi et al., 2022a). Tests with cellulose were performed at 220, 250, and 280 °C to provide a comparison with a lipid-free feedstock, as within this range a transition between HTC and HTL was previously identified observed for cellulose using thermodynamic data (Pecchi et al., 2022b). Details of these additional experiments are available in Appendix B of the SI.

Yields of each product phase, x, are denoted with Y_x . The yields of HC, the solid fraction obtained through vacuum filtration, and the aqueous phase (comprising water, dissolved organics, and some light biocrude that penetrates the filter paper) were determined gravimetrically. Gas yield was calculated based on the ideal gas law (Pecchi et al., 2022a). As the mass closure in the first run was within 11.8 % based on the dry feedstock amount, an additional step was taken in subsequent runs to reduce reactor loss, which improved mass closure to within 2.3 % or better for each run. To achieve this, the reactor is wiped with a premeasured mass of Kimwipes after collecting the final products. The amount of HC and liquid adsorbed by the Kimwipe is determined through gravimetric difference prior to and after drying of the wipe.

2.2. Solvent extraction and extract analysis

0.6 g of each as-carbonized HC is contacted with 20 mL of ethanol in a glass, PTFE-lined vial and agitated for 3 h at 60 rpm. After shaking, the vial's contents are filtered through cellulose paper and solids are further rinsed with 20 mL of ethanol. The filtrate and rinse are collected in a clean vial. The first vial and the filter paper with its HC are oven dried at 80 $^{\circ}$ C, overnight and weighed on a Shimadzu semi-microbalance (± 0.1 mg). The untreated, as carbonized HC is referred to as HC, the dried residue after filtration as PC (primary char), and the solubilized extracted material as SC (secondary char). This procedure is also applied to the untreated FW to separate the ethanol-insoluble from ethanol-soluble fraction.

The solubilized SC samples are mixed with excess MgSO₄ (approximately 100 mg MgSO₄ added to 1.5 mL of solvent containing SC). After mixing, the vials are centrifuged to remove residual water and the supernatant diluted to a ratio of 1:1 with ethanol. The solutions are analyzed on a Shimadzu Single Quadrupole Gas Chromatograph-Mass Spectrometer (GCMS-QP2020) with a Rxi-5MS capillary column. The initial column oven temperature is 40 °C with an injection temperature of 250 °C and a split ratio of 1:10 using ultra high purity helium (Airgas)

Waste Management 168 (2023) 281-289

 Table 1

 Proximate, ultimate, and calorimetric analysis of the raw FW, HC, PC and SC (average ± standard deviations of replicates); oxygen by difference, Italics indicate raw FW (un-extracted feedstock and solvent-extracted solid residue and extracted phase).

	Solid Yield [wt%]	Ash [wt% dry basis]	VM [wt% dry basis]	FC [wt% dry basis]	C [wt% dry, ash-free basis]	H [wt% dry, ash-free basis]	N [wt% dry, ash-free basis]	S [wt% dry, ash-free basis]	O [wt% dry, ash-free basis]	HHV [MJ/kg, dr basis]
As-Carbonize	d Hydrochar (HC)								
FW (raw)	n.a.	1.4 ± 0.0	$\textit{84.8} \pm \textit{0.8}$	13.8 ± 0.7	53.9 ± 2.2	8.9 ± 0.4	1.7 ± 0.1	0.4 ± 0.1	33.7 ± 2.3	26.0 ± 0.3
FW190-HC	58.8 ± 2.2	2.4 ± 0.9	85.2 ± 1.0	12.4 ± 0.1	72.7 ± 0.1	10.3 ± 0.0	1.9 ± 0.0	0.2 ± 0.0	12.6 ± 0.1	35.2 ± 0.2
FW220-HC	66.7 ± 2.5	1.5 ± 0.7	81.1 ± 0.9	17.6 ± 0.2	73.5 ± 0.3	9.7 ± 0.1	1.8 ± 0.0	0.2 ± 0.0	13.2 ± 0.3	35.2 ± 0.1
FW250-HC	66.8 ± 2.6	2.9 ± 0.9	77.7 ± 0.5	18.9 ± 0.0	74.4 ± 0.0	9.9 ± 0.1	1.9 ± 0.0	0.2 ± 0.0	10.8 ± 0.1	35.6 ± 0.1
FW280-HC	65.3 ± 2.5	2.1 ± 0.8	78.0 ± 0.8	19.8 ± 0.0	76.1 ± 0.2	9.9 ± 0.2	2.0 ± 0.0	0.1 ± 0.0	9.7 ± 0.3	36.1 ± 0.1
FW310-HC	63.7 ± 2.4	3.3 ± 0.1	75.8 ± 0.7	20.9 ± 0.7	77.4 ± 0.0	10.2 ± 0.1	2.0 ± 0.0	0.1 ± 0.0	7.1 ± 0.1	36.7 ± 0.1
FW340-HC	64.9 ± 2.5	1.5 ± 0.5	77.5 ± 0.3	21.4 ± 0.3	77.6 ± 0.3	10.2 ± 0.1	2.0 ± 0.0	0.1 ± 0.0	8.5 ± 0.3	37.1 ± 0.0
Solid Primary	Char Remaining	after Ethanol Extracti	on (PC)							
FW (solid)	58.7 ± 0.0	2.8 ± 0.1	81.7 ± 5.4	15.7 ± 5.6	45.8 ± 0.3	7.8 ± 0.2	2.5 ± 0.1	0.2 ± 0.0	41.0 ± 0.4	19.3 ± 0.3
FW190-PC	27.7 ± 2.2	3.6 ± 0.3	69.0 ± 0.4	29.7 ± 1.7	63.7 ± 0.3	7.4 ± 0.1	4.5 ± 0.2	0.3 ± 0.0	20.4 ± 0.4	28.5 ± 0.2
FW220-PC	31.9 ± 2.5	2.7 ± 0.2	54.6 ± 1.1	42.8 ± 0.9	66.8 ± 0.0	6.0 ± 0.1	4.1 ± 0.0	0.3 ± 0.0	20.1 ± 0.1	27.6 ± 0.1
FW250-PC	28.1 ± 2.6	2.8 ± 0.5	48.3 ± 0.4	48.9 ± 0.1	68.4 ± 0.1	5.6 ± 0.1	4.4 ± 0.0	0.2 ± 0.0	18.7 ± 0.2	27.8 ± 0.2
FW280-PC	30.4 ± 2.5	3.8 ± 1.1	46.1 ± 1.7	51.0 ± 1.6	71.0 ± 0.3	5.8 ± 0.1	4.3 ± 0.0	0.2 ± 0.0	14.9 ± 0.3	29.7 ± 0.2
FW310-PC	26.9 ± 2.4	3.2 ± 0.2	44.2 ± 0.1	52.7 ± 0.3	75.0 ± 0.2	6.1 ± 0.0	4.2 ± 0.0	0.2 ± 0.0	11.3 ± 0.2	32.1 ± 0.1
FW340-PC	21.9 ± 2.5	3.3 ± 0.2	43.2 ± 0.6	53.6 ± 0.8	76.7 ± 0.3	5.9 ± 0.1	4.2 ± 0.0	0.2 ± 0.0	9.7 ± 0.3	32.6 ± 0.1
	acted Secondary C									
FW	41.3 ± 0.0	-0.6 ± 0.2	89.2 ± 7.9	11.1 ± 8.2	65.4 ± 5.5	10.6 ± 1.0	0.6 ± 0.3	0.7 ± 0.1	23.4 ± 5.6	35.6 ± 0.9
(extract)										
FW190-SC	72.3 ± 2.2	2.0 ± 1.2	91.3 ± 1.4	5.8 ± 0.7	76.1 ± 0.2	11.4 ± 0.1	0.9 ± 0.1	0.2 ± 0.0	9.6 ± 0.2	37.8 ± 0.2
FW220-SC	68.1 ± 2.5	0.9 ± 1.0	93.6 ± 1.4	5.9 ± 0.5	76.7 ± 0.4	11.5 ± 0.2	0.7 ± 0.1	0.2 ± 0.0	10.0 ± 0.5	38.8 ± 0.2
FW250-SC	71.9 ± 2.6	2.9 ± 1.3	89.2 ± 0.7	7.1 ± 0.0	76.7 ± 0.1	11.6 ± 0.1	0.9 ± 0.1	0.1 ± 0.0	7.7 ± 0.2	38.6 ± 0.1
FW280-SC	69.6 ± 2.5	1.4 ± 1.2	91.9 ± 1.4	6.2 ± 0.7	78.3 ± 0.3	11.7 ± 0.3	1.0 ± 0.0	0.1 ± 0.0	7.5 ± 0.5	38.9 ± 0.1
FW310-SC	73.1 ± 2.4	3.3 ± 0.1	87.4 ± 1.0	9.2 ± 0.9	78.2 ± 0.1	11.6 ± 0.1	1.2 ± 0.0	0.1 ± 0.0	5.5 ± 0.1	38.4 ± 0.2
FW340-SC	78.1 ± 2.5	1.0 ± 0.6	87.1 ± 0.5	12.4 ± 0.5	77.9 ± 0.4	11.5 ± 0.1	1.4 ± 0.0	0.1 ± 0.0 0.1 ± 0.0	8.2 ± 0.4	38.3 ± 0.1

as a carrier gas flowing at 1 mL/min. After a 5-minute residence time the column temperature is increased at a rate of 2 $^{\circ}$ C min $^{-1}$ to 300 $^{\circ}$ C and held for 40 min. The mass spectrometer scans from 15 to 500 M/Z and data are recorded after a solvent cut time of 6 min. Peaks are identified using the embedded NIST library with a threshold of 70 % for the similarity; peaks with lower similarity are considered unidentified. Absolute areas are scaled to the maximum identified peak area (of all samples) to compute relative areas; this allows to compare the relative concentration of the same compound across different samples, but not the relative concentration of different compounds in the same sample.

2.3. Char analysis

Proximate analysis of both HC and PC samples are performed using a TA Instruments Simultaneous Thermal Analyzer 6500 and a TA Instruments TGA5500. 5–20 mg of sample is initially heated in high purity N_2 (Airgas) to 110 $^{\circ}\text{C}$ and held for 60 min to remove moisture. The temperature is then raised to 900 $^{\circ}\text{C}$ at 10 $^{\circ}\text{C}$ min and kept constant for 60 min to assess the volatile mass content. The flow of N_2 is then switched to dry air at 100 mL/min and the temperature is increased to 925 $^{\circ}\text{C}$ at a rate of 10 $^{\circ}\text{C}/\text{min}$. The temperature is again held for 60 min, the mass loss in this segment is attributed to the fixed carbon content of the sample; residual matter is termed ash. Derivative thermogravimetric curves (DTG) are computed from the time derivative of the mass loss in the volatile matter region, representing the pyrolysis step (only) as a gauge of thermal stability. Analyses were duplicated.

Ultimate analysis of the HC and PC are done on a Vario MACRO cube (Elementar) elemental analyzer to quantify elemental carbon, hydrogen, and nitrogen content. Oxygen is determined by difference. The analyzer is calibrated using sulfanilamide. Samples are run in triplicate.

The Higher Heating Values of the raw material (HHV $_{\rm Feed}$) and of the stabilized HC samples (HHV $_{\rm HC}$) are obtained using a 6200 Isoperibol Calorimeter equipped with a 6510 Water Handling system (Parr, USA) calibrated using benzoic acid. Each measured was triplicated.

Given the small sample amount available, the HHV of PC (HHV $_{PC}$) is estimated using Equation (1), a Dulong-type approximation (Hosokai et al., 2016), where the HHV $_{PC}$ is given in MJ kg $^{-1}$ and [C], [H], [O] are the PC's elemental contents:

$$HHV_{PC} = 0.338 \bullet [C] + 1.428 \bullet ([H] - \frac{1}{8[O]})$$
 (1)

SC properties (elemental composition, proximate analysis, HHV) are calculated by difference from HC and PC properties and yield assuming they are additive in nature. Every SC property, X_{SC} , (average) and its standard deviation, σ_{SC} , are calculated via:

$$X_{SC} = \frac{X_{HC} - X_{PC} \cdot Y_{PC}}{Y_{SC}}$$
 (2)

$$\sigma_{SC} = \frac{\sqrt{\sigma_{HC}^2 + (\sigma_{PC} \cdot Y_{PC})^2}}{Y_{SC}}$$
(3)

 $ER_{HC/PC/SC}$ represents the energy recovery relative to the HC, PC, or the SC phases respectively, determined via Equation (4):

$$ER_{HC/PC/SC} = Y_{HC/PC/SC} \cdot \frac{HHV_{HC/PC/SC}}{HHV_{Feed}} \cdot 100\%$$
 (4)

To assess changes in surface functional groups, the HC, PC, or SC are dried and mixed with approximately 200 mg of KBr at a $\sim 1\text{--}2$ wt% sample to KBr ratio. The mixture is pelletized under 6 MPa and analyzed on a Bruker Vertex 70 Fourier Transform Infrared Spectrometer (FT-IR). Infrared spectra are obtained using diffraction mode through the KBr pellet sample, performed using 64 scans at a 4 cm $^{-1}$ resolution over a wavenumber range of 4000 - 400 cm $^{-1}$. Spectra are baseline corrected and normalized to the O–H band between 3000 and 3800 cm $^{-1}$.

3. Results and discussion

A representative mixture of retail-level FW was used as a case study to understand transitions across the hydrothermal processing spectrum. US retail-level FW contains approximately 29% lipids, 60% carbohydrates, 10% proteins, and 1% ash on a dry basis, with a higher heating value (HHV $_{\rm feed}$) of 26 MJ kg $^{-1}$ (Buzby et al., 2014). The FW mixture fabricated here had a slightly greater energy content compared to prior hydrothermal studies using food waste (Akarsu et al., 2019; Maag et al., 2018; Mazumder et al., 2020). The difference in heating value can be attributed to the higher fraction of energy dense lipids comprising our waste feedstock.

3.1. Hydrothermal processing of food waste

The yields of HC, aqueous, and gaseous phases for raw FW and the HTC/HTL products are provided in Fig. 1, along with the solvent-extracted PC and SC yields. HTC at 220 °C is performed in triplicate to assess reproducibility, which results in standard deviations of 3.8 % for Y_{HC} , 5.5 % for Y_{liquid} , 5.6 % and for Y_{gas} . Operating at 190 °C results in the lowest Y_{HC} of 60%, while temperatures ≥ 220 °C produced a Y_{HC} between 64 and 66%. $Y_{aqueous}$ decreases with increasing operating temperature up to 250 °C, with a maximum yield of 36 wt% at 190 °C, which decreased to 17 – 28 wt% when treated between 220 and 340 °C. Y_{gas} increases almost linearly with temperature, in agreement with prior studies (Nizamuddin et al., 2017).

HHV_{HC} is reported in Table 1; HHV_{HC} are in line with previous work that used representative grocery store FW (Ul Sagib et al., 2019), but higher than prior FW hydrothermal studies that used FW with initial lower HHV (Akarsu et al., 2019; Mazumder et al., 2020; Sharma and Dubey, 2020). The HHV_{HC} increases with increasing treatment temperature, except for the hydrothermal runs performed at 190 °C (which has a HHV_{HC} greater than expected from the observed trend). A decreasing trend in HHV $_{HC}$ with temperature up to a minimum at 220 $^{\circ}C$ is observed in some prior work (Aragón-Briceño et al., 2017), whereas other works report a decreasing trend in HHV_{HC} with HTC treatment temperature without an apparent minimum (Berge et al., 2011; Zhang et al., 2014). Here we observed that at high temperatures (≥280 °C) the HHV_{HC} begins to plateau at \sim 36 MJ/kg. Because hydrolysis, recondensation and polymerization reactions occur both in series and in parallel, this shifts solid-liquid partitioning initially towards recondensation at moderate temperatures and towards the liquid phase at higher temperature, with associated char composition/characteristic shifts.

To better understand how HC evolves with temperature during HTC, we examine the HC thermal stability using thermogravimetric analysis. Fig. 2a provides DTG curves for the raw FW and the six HCs obtained when pyrolyzed in N_2 up to 800 °C (non-stacked version of these plots and TG curves are available in the SI). The raw FW has three distinct peaks in the volatile matter region, centered at \sim 200, \sim 300, and \sim 400 °C. The HCs display at most three DTG peaks, though not always aligned with the FW peaks. The first HC peak occurs at \sim 250 °C for samples carbonized at 220 °C and higher. The location of this first DTG peak shifts to higher temperatures as the HTC/HTL reaction temperature increases. The second HC peak is located at \sim 400 °C and is only present for HC produced at T \leq 250 °C, and its center shifts to lower temperatures as the HTC/HTL temperature increases. The last peak is centered at \sim 440 °C, it is absent for HC190, and its center shifts to higher temperatures with HTC/HTL temperature.

Mass loss at $\sim 250~^\circ\text{C}$ is primarily due to devolatilization of long chain fatty acids (LCFA) (Pecchi et al., 2022a), promising fuel precursors (Maghrebi et al., 2021). Similar to the trend in HHV $_{HC}$, mass loss rates in the DTG peak at $\sim 250~^\circ\text{C}$ increase with increasing hydrothermal processing temperatures between 220 and 280 $^\circ\text{C}$, and plateau to a constant mass loss rate for HCs formed between 280 and 340 $^\circ\text{C}$. This suggests that, up to 280 $^\circ\text{C}$, an increased fraction of LCFA is present in the HC

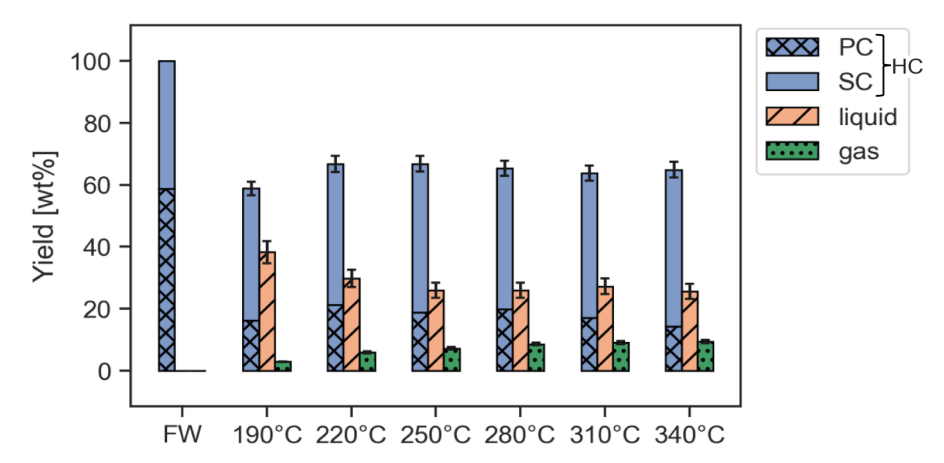


Fig. 1. Yields of HC, PC, SC and liquid and gaseous phases for untreated and hydrothermally processed FW. Error bars are estimated based on the triplicate run at 220 °C.

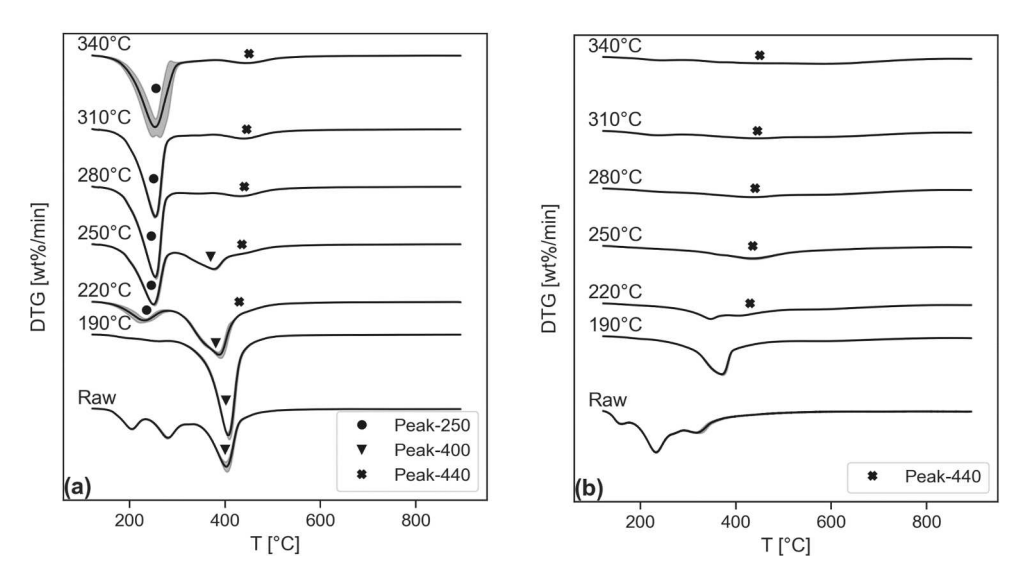


Fig. 2. DTG curves obtained under N2 atmosphere at 10 °C min⁻¹ for raw FW and six HC (plot a), and for the correspondent PCs (plot b). Solid lines represent the average value, shaded areas the standard deviation of replicates. Peaks named after approximate center-temperature. Proportions are maintained across the two plots and each curve to allow direct interpretation of changes in thermal stability across samples.

phase. The absence of a peak $\sim 250~^\circ\text{C}$ for HC produced at 190 $^\circ\text{C}$ suggests minimal lipid hydrolysis occurs below this temperature. Therefore, the trends in HHV $_{HC}$ cannot be entirely attributed to LCFA content in the HCs.

In contrast to how the peak at $\sim 250~^\circ C$ increases in mass loss rate as reaction temperature increases (Fig. 2a) a decrease in the peak mass loss rate at $\sim 400~^\circ C$ is observed as temperature increases between 190 and 250 $^\circ C$; HCs formed at HTC temperatures $\geq 280~^\circ C$ lack the DTG peak at $\sim 400~^\circ C$. The decreasing peak at $\sim 400~^\circ C$ in conjunction with an increasing peak at $\sim 250~^\circ C$ for HCs as temperature increases suggests that the less volatile HC fraction comprising the peak at $\sim 400~^\circ C$ reacts at higher HTC temperatures to produce a more volatile fraction responsible for the peak $\sim 250~^\circ C$, consistent with lipid hydrolysis to form LCFAs. The peak at $\sim 400~^\circ C$ is larger in HC formed at 190 $^\circ C$ versus the original FW feedstock, which suggests that lipids are concentrated in this HC relative to the original waste feedstock. The increase in lipid content is likely due to the initial dissolution of water-soluble organics, as indicated from the high Yaqueous in Fig. 1, increasing the relative concentration of lipids in the solid HC.

At temperatures \geq 280 °C, an additional DTG peak appears, located at \sim 440 °C, suggestive of the production of a more aromatic char (Li et al., 2020; Peng et al., 2023). The peak's center slightly shifts to higher

volatilization temperatures as HTC temperature increases, consistent with a higher degree of aromatization of the HC. Similar behavior was found for HTC of corn stover; while the raw corn stover had one DTG peak at $\sim 300\,^{\circ}\text{C}$, the HC produced at higher temperatures showed two distinct peaks, the first below 200 $^{\circ}\text{C}$ and the second around 400 $^{\circ}\text{C}$ (Mohammed et al., 2020).

3.2. SC extraction at different HTC/HTL conditions

Fig. 1 reports the HC yield, Y_{HC} , as the sum of its PC and SC, Y_{PC} and Y_{SC} , following ethanol extraction of the raw FW and HCs. The ethanol-soluble fraction in the raw FW and the Y_{SC} (~40 % in all cases) are comparable. The DTG profiles of the HCs and PCs in Fig. 2 (plots a and b, respectively) show that extraction eliminates peaks at ~ 250 and ~ 400 °C, associated with the presence of LCFA and leaves behind the (small) peak at ~ 440 °C, attributed to a more aromatic char that is not ethanol-soluble. The presence of this DTG peak and of another between 500 and 600 °C (also suggestive of a more aromatic phase) is observed in FTIR analysis (Fig. 3a). FTIR spectra of HC show a decreasing semi-quantitative trend for aliphatic carbon vibrations (~2925 and 2850 cm $^{-1}$ for CH₃ and CH₂, respectively) and an increasing amount of aromatic vibrations (~800 cm $^{-1}$) with increasing temperature, in

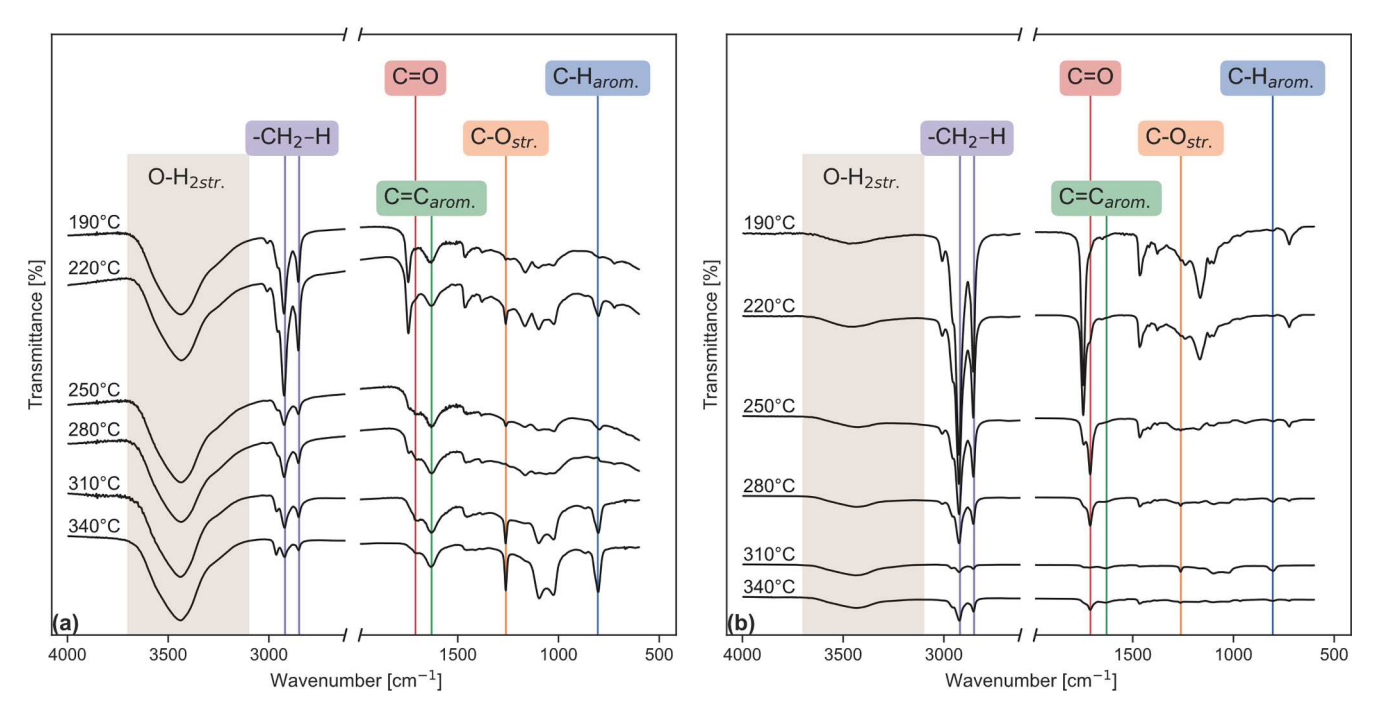


Fig. 3. IR spectra for (a) HC obtained from HTC of FW and (b) SC obtained from ethanol extracted of those HC.

agreement with an enhanced aromatization of the HC matrix. Interestingly, the DTG peaks of the ethanol-extracted raw FW and of the PC produced at 220 $^{\circ}\text{C}$ also indicate that a significant fraction of the lipids is not converted into LCFA. These unreacted lipids remain on the PC, as ethanol cannot extract them.

These changes in the HCs upon ethanol extraction are echoed in the proximate and ultimate analyses (Table 1). While the raw and ethanol-extracted FW have similar compositions, HCs and their respective PCs and SCs differ significantly. Ethanol preferentially extracts VM in the HCs at an increased extent with increasing HTC temperature. This supports the idea that most ethanol-insoluble compounds (e.g., triglycerides) in the raw FW are converted into more ethanol-soluble ones at higher HTC/HTL temperature (e.g., LCFA).

As Table 1 shows, the PCs have a lower elemental C content than their respective SCs, in agreement with previous work where SC extraction showed a higher HHV than the HCs and PCs and, thus, a higher C content (Lucian et al., 2018). The C content of all SC is between 76 and 78 %, with higher values at higher HTC/L temperatures. While the data show a slightly parabolic trend (the C content for SC at 340 is 77.9% versus 78.2% and 78.3% at 340, 310 and 280 °C, respectively). the differences between C composition between successive SCs are not statistically significant (p < 0.05, two-tailed t-tests between neighboring data points). The jump in C content from 76.7 % to 78.3 % for SCs produced at 250 and 280 °C is highly statistically significant (p = 0.0009). This is consistent with the presence of a large fraction of fatty acids that undergo amidation (which reduces the C fraction by including N in the chain) and a minor fraction of compounds (ketones, alcohols, furfurals, etc.) that undergo decarboxylation and condensation with increasing temperature (Leng et al., 2020). Amidation outperforms the Maillard reaction (and therefore the decarboxylation of its products) at higher temperatures (Fan et al., 2020; Wang et al., 2018). Similarly, each successive PC sees a 2-5% increase in C content (each increase is statistically significantly different, p < 0.05), suggesting an increased extent of dehydration and decarboxylation of the polyaromatic solid phase with temperature (Kumar et al., 2020).

Temperature has a minor effect on N partitioning to the HC phase versus the HTC/L aqueous phase (Idowu et al., 2017). Interestingly, N favors the PC; PC has a \sim 4-fold greater N content than SC. This suggests that nitrogen fixation mechanisms are enhanced during HTC, but likely

via different mechanisms. For carbohydrate-rich biomass at medium HTC temperatures (180–240 °C), Maillard and Mannich reactions favor the production of intermediate hemiaminals (LeClerc et al., 2022) that further promote N-incorporation in the HC in the form of pyrrole, pyridine, and quaternary-N (He et al., 2015; Leng et al., 2021; Wang et al., 2021). At higher temperatures, amidation of LCFA is favored over the Maillard reaction, decreasing pyrazines in the bio-oil in favor of fatty acid amides (Fan et al., 2020; Wang et al., 2018). This agrees with the results of this study; the N in the PC (mainly fixated as pyrrole, pyridine, and quaternary-N) mildly decreases with temperature, while the SC N-content mildly increases (Table 1), due to an increased production of fatty acid amines that are readily extracted by ethanol.

A van Krevelen diagram (Fig. 4) highlights the chemical transformations HCs, PCs, and SCs undergo during HTC/L. As hydrothermal treatment temperatures increase, HC compositions increasingly fall between that of coal and crude oil. After ethanol extraction, PC compositions appear more coal-like, while SC compositions increasingly represent a crude oil, creating two separate phases with more

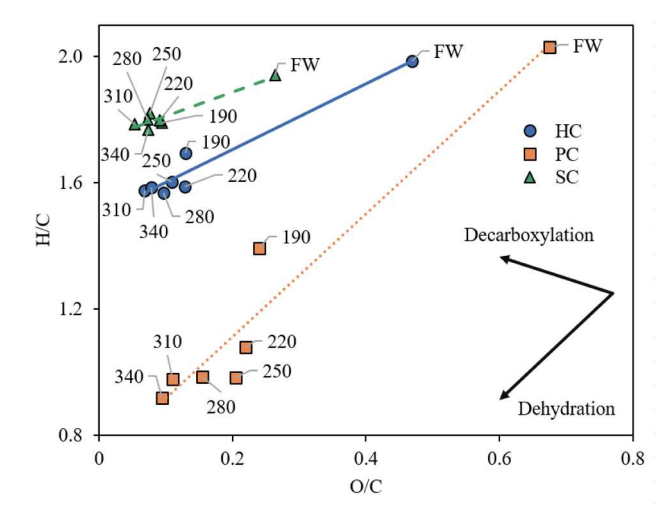


Fig. 4. Van krevelen diagram for hcs, pcs, and scs.

established valorization paths compared to the hybrid HC.

Fig. 1 indicates that – up to 250 °C – increasing the processing temperature favors the partitioning of aqueous phase compound onto the HC. Fig. 5 shows the HHV and ER of raw FW, HC, and their separated products. In the raw FW, the difference between $\rm ER_{PC}$ and $\rm ER_{SC}$ is minimal, even though the HHV $_{SC}$ is almost doubled compared to HHV $_{PC}$. While $\rm Y_{PC} > \rm Y_{SC}$, the extract is mainly composed of high-energy lipids (Fig. 6) and the insoluble fraction is (presumably) enriched in oxygenated carbohydrates and proteins. The situation changes after HTC at 190 °C; both HHV $_{PC}$ and HHV $_{SC}$ increase (HHV $_{PC}$ to a greater extent) but $\rm Y_{PC}$ is reduced in favor of $\rm Y_{SC}$. This increases ER $_{SC}$, which is matched by a reduction in ER $_{PC}$. For runs at 220 and 250 °C, both $\rm Y_{PC}$ and $\rm Y_{SC}$ increase, with slightly lower HHV $_{PC}$ compared to the run at 190 °C. At these moderate temperatures HHV $_{SC}$ increases. Above 250 °C, HHV $_{PC}$ again increases, while HHV $_{SC}$ decreases.

The trends in Fig. 5 seem to indicate the presence of two main regimes above and below 250 °C. This transition temperature seems to represent a local optimum to maximize the ER_{SC}. Below 250 °C, HTC increases the Y_{HC} and less markedly HHV $_{HC}$ (with a drop at 220 °C). The increase in HHV $_{HC}$ is first due to an increase in the Y_{SC} , and second to a greater HHV $_{SC}$ than HHV $_{PC}$, as the latter decreases. Above 250 °C – when we are in the so-called HTL regime – the increase in HHV $_{HC}$ is due to an increase in HHV $_{PC}$ rather than HHV $_{SC}$ (which slightly decreases, as shown in Fig. 4). Since HHV $_{PC}$ increases up to 310 °C, the ER $_{SC}$ is lower than that at 250 °C. Indeed, a local maximum in the ER $_{SC}$ is found at 250 °C, in agreement with previous studies (Lucian et al., 2018). At 340 °C, HHV $_{PC}$ and HHV $_{SC}$ are close to those obtained at 310 °C, but due to a small Y_{PC} value, the ER $_{SC}$ is the highest.

To further support this discussion, GC–MS identified compounds in the extracted SC phases are shown in Fig. 6. The SC produced at 190 °C mainly contains one short-chained unidentified compound and small amounts of palmitic and oleic acids. For SC produced at 220 °C, LCFA begin to appear. SCs produced at temperatures \geq 250 °C, are concentrated in LCFA (e.g., palmitic, oleic, and stearic acids), which is expected as the process enters the liquefaction regime (Li et al., 2020; Lucian et al., 2018). This agrees with prior results from SC produced at 250 °C from feedstocks with varying lipid contents (Pecchi et al., 2022a), where LCFA were the major compounds found in SC regardless of the amount of lipids present in the feedstock.

The data indicate a rather discrete nature for lipid conversion into LCFA, which is hindered up to 220 $^{\circ}\text{C}$ yet occurs rather completely from 250 $^{\circ}\text{C}$ upwards. This is vastly different than observations concerning

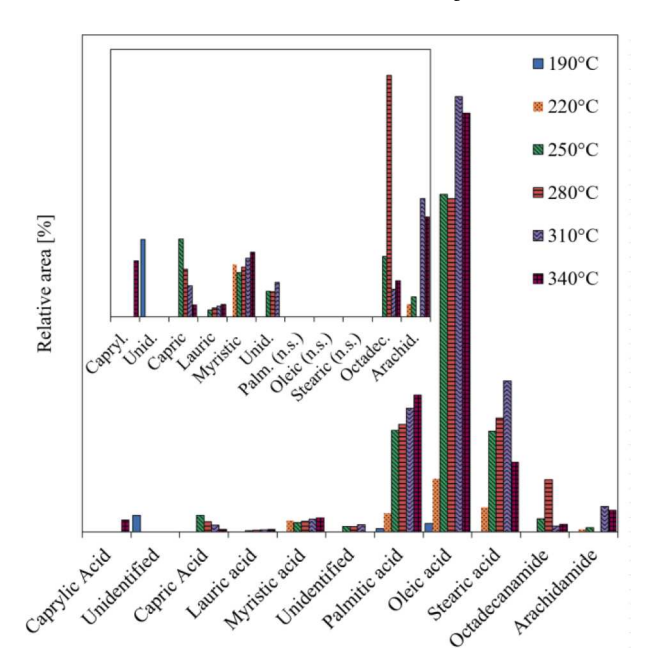


Fig. 6. Relative areas (to the maximum identified peak) of compounds identified using GC–MS in SC extracted with ethanol from HCs. The inset shows compounds with lower areas, excluding prominent peaks (palmitic, oleic, and stearic acid) to enhance visibility of minor components.

the PC phase, whose proximate and elemental composition gradually change with hydrothermal reaction severity. Significant amounts of octadecanamide and arachidamide are found in SC produced at \geq 250 °C and \geq 280 °C, respectively, which agrees with the assertion that amidation of LCFA is favored at higher temperatures (Fan et al., 2020; Wang et al., 2018). The GC–MS results align with the long chain organic acid functionality found in SC through FT-IR analysis (Fig. 3). SC peaks tend to decrease in magnitude with increasing temperature; the primary ones that remain at 340 °C are attributed to CH₃, CH₂, and C=O vibrations (~2925, 2850, 1250 cm $^{-1}$) and are typical of LCFAs.

The aim of this work was to investigate the HTC/HTL transition for a problematic biomass, food waste, as a case study; we recognize its limitations in being a high-lipid feedstock. While a full investigation of this transition behavior for other feedstocks is beyond the scope of this work, we ran additional HTC/HTL and SC extraction experiments on

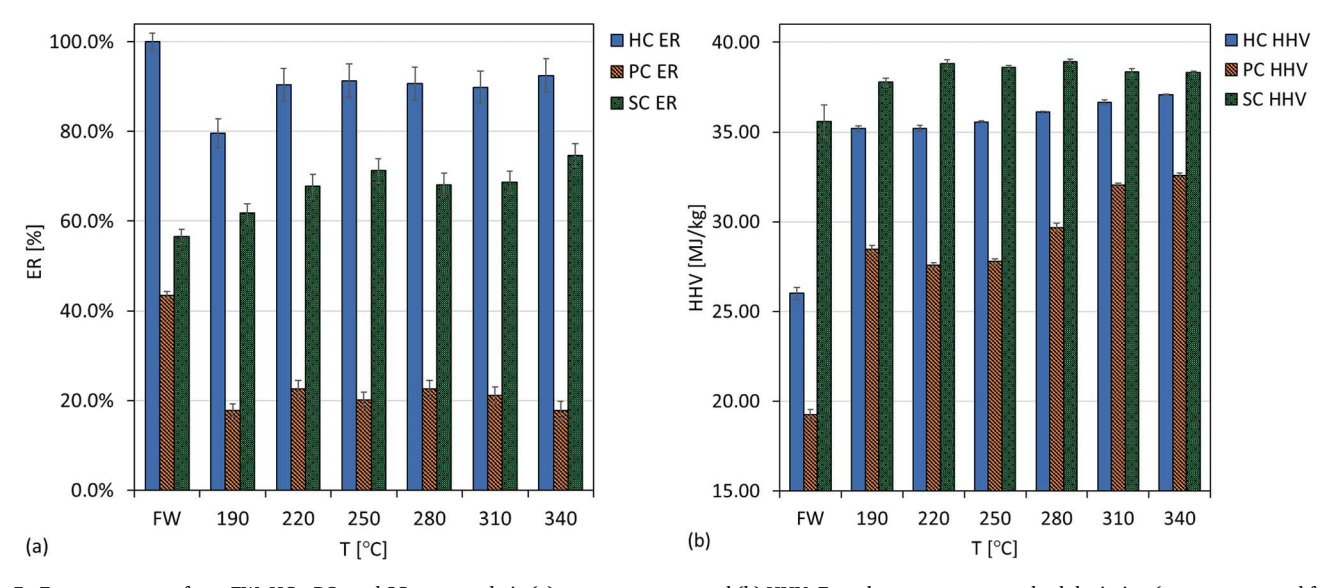


Fig. 5. Energy content of raw FW, HCs, PCs and SC expressed via (a) energy recovery and (b) HHV. Error bars represent standard deviation (error propagated for ER calculation).

cellulose at 220, 250, 280 °C (details reported in SI). The composition of cellulose SC (with Y_{SC} in the order of 13 ± 1 %) indicates that a similar transition occurs at 250 °C for cellulose. This indicates that although the primary products observed in SC from the FW are lipid-driven, that the carbohydrate fraction of the feedstock also shows a transition between HTC and HTL around 250 °C. For cellulose, HTC transitions to HTL where the conversion of 5-HMF into 4-oxopentanoic acid stops being kinetically limited, which agrees with previous work that indicates the presence of a thermodynamic discontinuity found at 255 °C for HTC/HTL of cellulose using differential scanning calorimetry (DSC) (Pecchi et al., 2022b).

In summary, if the aim of HTC/L is to produce LCFA from high lipid content wastes, selecting a temperature around 250 $^{\circ}\text{C}$ could reduce the energy cost of the process while maximizing the SC yield and minimizing its N and S content. Conversely, if the goal is to maximize 5-HMF production from cellulosic feedstocks, temperatures below this transition point should be employed. Y_{SC} from cellulose HC extracted with ethanol is significantly smaller that its FW counterpart, reminding us that the economic viability of scaling up such HTC/HTL process is feedstock dependent.

3.3. Transition between processes

The investigation of the product distribution and the HC proximate and ultimate analyses suggests a predominantly linear degradation pathway across HTC and HTL regimes as a function of temperature. In general, higher temperatures produce more gas, less liquid, and similar amounts of a progressively more carbonized and hydrogenated HC. The HC comprises a progressively more carbonaceous PC and more hydrogenated SC. The trends observed agree with prior assertions that temperature is correlated with the extent of dehydration, decarbonylation, and decarboxylation reactions.

However, a different picture emerges from PC and SC yields and compositions. Below 250 °C, HTC mostly increases the HHV_{SC} and decreases HHV_{PC}. This suggests HTC reactions involving a feedstock with a high lipid fraction tend to hydrolyze the lipids, increasing both yield and energy content of SC. For cellulosic feedstocks (see SI), SC yields are considerably smaller, yet their composition still indicates that $\sim 250~^\circ\text{C}$ is a thermodynamic discontinuity – in agreement with prior DSC investigations (Pecchi et al., 2022b) – after which full conversion of 5-HMF into smaller products occurs.

The hydrolysis of lipids into LCFA starts around 220 °C at slower rates, but stops being kinetically limited from 250 °C onward (Holliday et al., 1997; Johnson and Tester, 2013). The presence of DTG peaks attributed to LCFA (the peak at \sim 250 °C in Fig. 2) and the GC–MS analysis of SC (Fig. 6) suggest that 250 °C is a threshold for meaningful hydrolysis of lipids into LCFA. Above 250 °C, no significant gain in HC yield occurs by increasing temperature as condensation, polymerization, and amidation rates increase.

The local peak in the ER of SCs at 250 °C (Fig. 5) suggests that 250 °C is the lowest temperature at which lipids completely hydrolyze, but at which polymerization, condensation, gasification, and amidation reaction rates are relatively low. At 280 °C and above, HTL reduces the HHV $_{\rm SC}$ and ER $_{\rm SC}$, while HHV $_{\rm PC}$ strongly increases and ER $_{\rm PC}$ is mostly unaffected. This implies a change in the chemical mechanism compared from HTC to HTL as oil molecules react forming a more aromatic phase with lower hydrogen content. This phase has a reduced HHV compared to the more hydrogenated SC, explaining the lower HHV $_{\rm SC}$; condensation and polymerization of dissolved organics on the PC surface are likely responsible for the increased HHV and hydrogen content of the PC phase.

The present work suggests that hydrothermal processing of high lipid-content feedstocks around 250 $^{\circ}$ C maximizes the lipid conversion to LCFA and reduces subsequent recondensation and repolymerization to PC and their amidation to fatty acids amides. Maintaining this relatively low HTL temperature can reduce the energy cost of the process

compared to adopting traditional higher temperature HTL conditions.

4. Conclusions

A series of hydrothermal carbonization (HTC) and liquefaction (HTL) reactions were performed on food waste between 190 and 340 $^{\circ}\text{C}$ for 1 h to probe the transition between HTC and HTL as a function of temperature. Select additional experiments on cellulose at 220, 250, and 280 $^{\circ}\text{C}$ were used to confirm the existence of a transition for a non-lipidic feedstock.

While a smooth transition between HTC and HTL seems to occur when we examine the product distribution and hydrochar heating value and elemental composition, a different picture is instead provided by the compositional analysis of the primary and the secondary char phase.

While cellulose sees low secondary char yields, SC of food waste accounts for more than 50 wt% of the HC. From 220 °C onward, HTC reactions of this high lipid feedstock begin to hydrolyze the lipid phase, generating more energy-dense secondary char that coalesces on the primary char. Above 250 °C, the hydrolysis of lipids into long chain fatty acids stops being kinetically limited and the energy recovered in the secondary char phase shows a local maximum. From 280 °C and above, oil molecules react to form fatty acid amides (increasing the secondary char nitrogen content) and a more aromatic phase with lower hydrogen content and reduced heating value compared to the more hydrogenated secondary char phase. This phase condenses and (re)polymerizes on the primary char surface, increasing the primary char heating value and hydrogen content at the cost of the secondary char yield.

Broadly speaking, for hydrothermal conversion of high lipid wastes, temperatures around 250 $^{\circ}\text{C}$ appear to maximize the lipid conversion to long chain fatty acids and reduce their recondensation and repolymerization to solid primary char. Despite commonly held beliefs that higher temperatures are required to enter into the liquefaction regime, for high lipid feedstocks it may be possible to reduce process energy consumption by maintaining lower process temperatures. Furthermore, extracting the secondary char phase using ethanol recovers around 70 % of the initial energy in the feedstock in the form of a high heating value liquid fuel precursor.

Declaration of Competing Interest

The authors declare that they have no known competing financial interests or personal relationships that could have appeared to influence the work reported in this paper.

Data availability

Data will be made available on request.

Acknowledgements

The authors thank Laura G. Falls for her assistance in compiling the food waste mixture.

Funding

This work was partially supported by a Hatch Grant under accession number 1021398 from the USDA National Institute of Food and Agriculture and by the National Science Foundation under grant CBET-2031916.

Appendix A. Supplementary material

Supplementary data to this article can be found online at https://doi.org/10.1016/j.wasman.2023.06.009.

References

- Akarsu, K., Duman, G., Yilmazer, A., Keskin, T., Azbar, N., Yanik, J., 2019. Sustainable valorization of food wastes into solid fuel by hydrothermal carbonization. Bioresour. Technol. 292, 121959 https://doi.org/10.1016/j.biortech.2019.121959.
- Akbari, M., Oyedun, A.O., Kumar, A., 2020. Techno-economic assessment of wet and dry torrefaction of biomass feedstock. Energy 207, 118287. https://doi.org/10.1016/j. energy.2020.118287.
- Aragón-Briceño, C., Ross, A.B., Camargo-Valero, M.A., 2017. Evaluation and comparison of product yields and bio-methane potential in sewage digestate following hydrothermal treatment. Appl. Energy 208, 1357–1369. https://doi.org/10.1016/j. apenergy.2017.09.019.
- Beims, R.F., Hu, Y., Shui, H., Xu (Charles), C., 2020. Hydrothermal liquefaction of biomass to fuels and value-added chemicals: products applications and challenges to develop large-scale operations. Biomass Bioenergy 135. https://doi.org/10.1016/j. biombioe.2020.105510.
- Berge, N.D., Ro, K.S., Mao, J., Flora, J.R.V., Chappell, M.A., Bae, S., 2011. Hydrothermal carbonization of municipal waste streams. Environ. Sci. Technol. 45, 5696–5703. https://doi.org/10.1021/es2004528.
- Buzby, J.C., Farah-Wells, H., Hyman, J., 2014. The estimated amount, value, and calories of postharvest food losses at the retail and consumer levels in the United States. SSRN Journal. https://doi.org/10.2139/ssrn.2501659.
- EPA, 2018. 2018 Wasted Food Report Estimates of generation and management of wasted food in the United States in 2018 (No. 530- R-20- 004). EPA - Office of Resource Conservation and Recovery.
- E.E. Agency Bio-waste in Europe: turning challenges into opportunities 2020 Publications Office LU Eurostat, 2022. Amounts of food waste at EU level.
- Fan, Y., Hornung, U., Raffelt, K., Dahmen, N., 2020. The influence of lipids on the fate of nitrogen during hydrothermal liquefaction of protein-containing biomass. J. Anal. Appl. Pyrol. 147, 104798 https://doi.org/10.1016/j.jaap.2020.104798.
- Appl. Pyrol. 147, 104798 https://doi.org/10.1016/j.jaap.2020.104798.

 He, C., Wang, K., Yang, Y., Amaniampong, P.N., Wang, J.-Y., 2015. Effective nitrogen removal and recovery from dewatered sewage sludge using a novel integrated system of accelerated hydrothermal deamination and air stripping. Environ. Sci. Technol. 49, 6872–6880. https://doi.org/10.1021/acs.est.5b00652.
- Holliday, R.L., King, J.W., List, G.R., 1997. Hydrolysis of vegetable oils in sub- and supercritical water. Ind. Eng. Chem. Res. 36, 932–935. https://doi.org/10.1021/ ie960668f.
- Hosokai, S., Matsuoka, K., Kuramoto, K., Suzuki, Y., 2016. Modification of Dulong's formula to estimate heating value of gas, liquid and solid fuels. Fuel Process. Technol. 152, 399–405. https://doi.org/10.1016/j.fuproc.2016.06.040.
- Idowu, I., Li, L., Flora, J.R.V., Pellechia, P.J., Darko, S.A., Ro, K.S., Berge, N.D., 2017. Hydrothermal carbonization of food waste for nutrient recovery and reuse. Waste Manag. 69, 480–491. https://doi.org/10.1016/j.wasman.2017.08.051.
- Johnson, M.C., Tester, J.W., 2013. Lipid transformation in hydrothermal processing of whole algal cells. Ind. Eng. Chem. Res. 52, 10988–10995. https://doi.org/10.1021/ iod00976w
- Kumar, A., Saini, K., Bhaskar, T., 2020. Hydochar and biochar: production, physicochemical properties and techno-economic analysis. Bioresour. Technol. 310, 123442 https://doi.org/10.1016/j.biortech.2020.123442.
- Lachos-Perez, D., César Torres-Mayanga, P., Abaide, E.R., Zabot, G.L., De Castilhos, F., 2022. Hydrothermal carbonization and Liquefaction: differences, progress, challenges, and opportunities. Bioresour. Technol. 343, 126084 https://doi.org/ 10.1016/j.biortech.2021.126084.
- LeClerc, H.O., Atwi, R., Niles, S.F., McKenna, A.M., Timko, M.T., West, R.H., Teixeira, A. R., 2022. Elucidating the role of reactive nitrogen intermediates in hetero-cyclization during hydrothermal liquefaction of food waste. Green Chem 24 (13), 5125–5141.
- Leng, L., Zhang, W., Peng, H., Li, H., Jiang, S., Huang, H., 2020. Nitrogen in bio-oil produced from hydrothermal liquefaction of biomass: a review. Chem. Eng. J. 401, 126030 https://doi.org/10.1016/j.cej.2020.126030.
- Leng, L., Yang, L., Leng, S., Zhang, W., Zhou, Y., Peng, H., Li, H., Hu, Y., Jiang, S., Li, H., 2021. A review on nitrogen transformation in hydrochar during hydrothermal carbonization of biomass containing nitrogen. Sci. Total Environ. 756, 143679 https://doi.org/10.1016/j.scitotenv.2020.143679.
- Li, J., Li, L., Suvarna, M., Pan, L., Tabatabaei, M., Ok, Y.S., Wang, X., 2022. Wet wastes to bioenergy and biochar: a critical review with future perspectives. Sci. Total Environ. 817, 152921 https://doi.org/10.1016/j.scitotenv.2022.152921.
- Li, Y., Liu, H., Xiao, K., Jin, M., Xiao, H., Yao, H., 2020. Combustion and pyrolysis characteristics of hydrochar prepared by hydrothermal carbonization of typical food

- waste: influence of carbohydrates, proteins, and lipids. Energy Fuel 34, 430–439. https://doi.org/10.1021/acs.energyfuels.9b02940.
- Lucian, M., Volpe, M., Gao, L., Piro, G., Goldfarb, J.L., Fiori, L., 2018. Impact of hydrothermal carbonization conditions on the formation of hydrochars and secondary chars from the organic fraction of municipal solid waste. Fuel 233, 257–268. https://doi.org/10.1016/j.fuel.2018.06.060.
- Maag, A.R., Paulsen, A.D., Amundsen, T.J., Yelvington, P.E., Tompsett, G.A., Timko, M. T., 2018. Catalytic hydrothermal liquefaction of food waste using cezrox. Energies 11, 1–14. https://doi.org/10.3390/en11030564.
- Maghrebi, R., Buffi, M., Bondioli, P., Chiaramonti, D., 2021. Isomerization of long-chain fatty acids and long-chain hydrocarbons: a review. Renew. Sustain. Energy Rev. 149, 111264 https://doi.org/10.1016/j.rser.2021.111264.
- Mazumder, S., Saha, P., McGaughy, K., Saba, A., Reza, M.T., 2022. Technoeconomic analysis of co-hydrothermal carbonization of coal waste and food waste. Biomass Convers. Biorefin. 12 (1), 39–49.
- Mohammed, I.S., Na, R., Kushima, K., Shimizu, N., 2020. Investigating the effect of processing parameters on the products of hydrothermal carbonization of corn stover. Sustainability (Switzerland) 12 (12), 5100. https://doi.org/10.3390/su12125100.
- Nizamuddin, S., Baloch, H.A., Griffin, G.J., Mubarak, N.M., Bhutto, A.W., Abro, R., Mazari, S.A., Ali, B.S., 2017. An overview of effect of process parameters on hydrothermal carbonization of biomass. Renew. Sustain. Energy Rev. 73, 1289–1299. https://doi.org/10.1016/j.rser.2016.12.122.
- Özçimen, D., İnan, B., Koçer, A.T., Bostyn, S., Gökalp, İ., 2022. Hydrothermal carbonization processes applied to wet organic waste streams. Int. J. Energy Res. 46, 16109–16126. https://doi.org/10.1002/er.8304.
- Pauline, A.L., Joseph, K., 2020. Hydrothermal carbonization of organic wastes to carbonaceous solid fuel – a review of mechanisms and process parameters. Fuel 279, 118472. https://doi.org/10.1016/j.fuel.2020.118472.
- Pecchi, M., Baratieri, M., Goldfarb, J.L., Maag, A.R., 2022a. Effect of solvent and feedstock selection on primary and secondary chars produced via hydrothermal carbonization of food wastes. Bioresour. Technol. 348, 126799 https://doi.org/ 10.1016/j.biortech.2022.126799.
- Pecchi, M., Cascioli, A., Maag, A.R., Goldfarb, J.L., Baratieri, M., 2022b. Uncovering the transition between hydrothermal carbonization and liquefaction using differential scanning calorimetry. Fuel Process. Technol. 235, 107349 https://doi.org/10.1016/ i.fuproc.2022.107349.
- Peng, J., Kang, X., Zhao, S., Zhao, P., Ragauskas, A.J., Si, C., Xu, T., Song, X., 2023. Growth mechanism of glucose-based hydrochar under the effects of acid and temperature regulation. J. Colloid Interface Sci. 630, 654–665. https://doi.org/10.1016/j.jcis.2022.10.044.
- Sharma, H.B., Dubey, B.K., 2020. Co-hydrothermal carbonization of food waste with yard waste for solid biofuel production: Hydrochar characterization and its pelletization. Waste Manag. 118, 521–533. https://doi.org/10.1016/j. wasman.2020.09.009.
- Ul Saqib, N., Sarmah, A.K., Baroutian, S., 2019. Effect of temperature on the fuel properties of food waste and coal blend treated under co-hydrothermal carbonization. Waste Manag. 89, 236–246. https://doi.org/10.1016/j. wasman 2019 04 005
- Wang, R., Lei, H., Liu, S., Ye, X., Jia, J., Zhao, Z., 2021. The redistribution and migration mechanism of nitrogen in the hydrothermal co-carbonization process of sewage sludge and lignocellulosic wastes. Sci. Total Environ. 776, 145922 https://doi.org/ 10.1016/j.scitotenv.2021.145922.
- Wang, T., Zhai, Y., Zhu, Y., Peng, C., Xu, B., Wang, T., Li, C., Zeng, G., 2018. Influence of temperature on nitrogen fate during hydrothermal carbonization of food waste. Bioresour. Technol. 247, 182–189. https://doi.org/10.1016/j.biortech.2017.09.076.
- Xu, D., Savage, P.E., 2014. Characterization of biocrudes recovered with and without solvent after hydrothermal liquefaction of algae. Algal Res. 6, 1–7. https://doi.org/ 10.1016/j.algal.2014.08.007.
- Yang, J., (Sophia) He, Q., Yang, L., 2019. A review on hydrothermal co-liquefaction of biomass. Appl. Energy 250, 926–945.
- Zhang, X., Li, X., Li, R., Wu, Y., 2020. Hydrothermal carbonization and liquefaction of sludge for harmless and resource purposes: a review. Energy Fuel 34, 13268–13290. https://doi.org/10.1021/acs.energyfuels.0c02467.
- Zhang, J., Lin, Q., Zhao, X., 2014. The hydrochar characters of municipal sewage sludge under different hydrothermal temperatures and durations. J. Integr. Agric. 13, 471–482. https://doi.org/10.1016/S2095-3119(13)60702-9.
- Zhuang, X., Liu, J., Zhang, Q., Wang, C., Zhan, H., Ma, L., 2022. A review on the utilization of industrial biowaste via hydrothermal carbonization. Renew. Sustain. Energy Rev. 154, 111877 https://doi.org/10.1016/j.rser.2021.111877.